


RESEARCH

Open Access



Colorless and unidirectional diffractive-type solar concentrators compatible with existing windows

Dewei Zhang^{1,3†}, Zhenghao Guo^{1†}, Chun-Ting Xu¹, Jianqing Li^{1,3}, Yan-Qing Lu^{1,2*} and Wei Hu^{1,2,3*} 

[†]Dewei Zhang and Zhenghao Guo contributed equally to this work.

*Correspondence: yqlu@nju.edu.cn; huwei@nju.edu.cn

¹ National Laboratory of Solid State Microstructures, Key Laboratory of Intelligent Optical Sensing and Manipulation, College of Engineering and Applied Sciences, Nanjing University, Nanjing 210093, China

² Jiangsu Physical Science Research Center, Nanjing University, Nanjing 210023, China

³ Wujin-NJU Institute of Future Technology, Changzhou 213100, China

Abstract

Solar concentrators laterally converge solar energy to the side of architectural glass and are attractive candidates for building-integrated photovoltaics. Present available luminescent-type and scattering-type solar concentrators suffer from omnidirectional waveguide induced low efficiency, coloring/hazing restrained aesthetic quality, and poor compatibility with existing architectural glass. Here, we propose a diffractive solar concentrator via directly coating cholesteric liquid crystal (CLC) layers onto the architectural glass. The stacked CLC layers with submicron lateral periodic alignment enable broadband and unidirectional waveguiding inside the glass, and thus supply a high-efficient platform for transmissive solar energy capturing with merits of high aesthetic quality and economic viability. A 1-inch-diameter prototype powers a 10-mW fan outdoors, and a typical 2-m-wide window is calculated to concentrate solar energy by 50 times. The design is expected to bring a global terawatt-scale green energy supply and billion-ton annual carbon emission reduction, meeting with the sustainable development of human society.

Keywords: Diffractive optics, Solar concentrators, Liquid crystals

Introduction

With the massive population growth and rapid urbanization in contemporary society, an increasing number of tower blocks and super high-rise buildings have emerged in urbans [1]. Drones driving low-altitude economies further accelerate the three-dimensional (3D) development of cities [2, 3]. The sharp increase in population density promotes production and cooperation efficiency, accompanied by increasingly evident resource and energy consumption. Thermal and nuclear power stations face challenges of environmental pollution and nuclear waste leakage risks, whereas renewable photovoltaic, wind power and hydroelectric energy generation have to occupy a large amount of space and set near corresponding sources [4, 5]. The centralized power supply additionally suffers from high transmission loss. Therefore, newly proposed building integrated photovoltaics, which incorporate solar energy capture into building facades, have drawn intensive attention to net-zero energy buildings [6, 7]. Glass windows are widely used in modern architectures for comfortable living and working conditions. They are

usually placed on sunny buildings to optimize natural lighting and heating [8, 9]. The integration of photovoltaic technologies with architectural glass would provide a promising strategy for green buildings and a sustainable society.

For existing photovoltaic techniques, including amorphous silicon cells, organic photovoltaics, gallium arsenide, dye-sensitized, and perovskite solar cells, their opacity and fragility impede the replacement of architectural glass [10, 11]. To solve these problems, solar concentrators have been developed to laterally concentrate solar energy and then capture it with photovoltaic cells fixed on the side of architectural glass. Luminescent and scattering types have been reported [12–14]. For the former, fluorescent materials such as organic dyes, polymers, quantum dots, perovskites, or carbon quantum dots are embedded in glass to form a waveguide for illuminated light [15, 16]. For the latter, an embedded light-scattering medium scatters part of the incident light into the waveguide, which is harvested by thin photovoltaic cells attached to the edges of the glass [17]. Despite the enhanced adaptability with present windows, such solar concentrators still face several critical challenges: (i) As light with only a propagation direction exceeding the critical angle for total internal reflection (TIR) can be collected by the waveguide, the omnidirectional fluorescence illumination and light scattering restrict the efficiency of solar concentration [18, 19]; (ii) the limited absorption and fluorescent bands with respect to the solar spectrum not only reduce the efficiency but also induce a colored transparency, making the corresponding glass unable to match the aesthetic requirements [20, 21]; meanwhile, the scattering type suffers from intrinsic visible haziness, thus hindering many applications requiring an unobstructed view [17]; and (iii) the embedded functional layers cannot be added to the existing windows, and photovoltaic cells are required on all edges of architectural glass, making the strategy suffer from complicated manufacturing and cost inefficient [22, 23]. It is an urgent task to develop new technique overcoming all these hurdles. Polarization volume grating is a circular polarization dependent optical device. It is transmissive to one circular polarization and meanwhile unidirectionally diffracts the opposite one into the glass substrate to form a waveguide [24, 25]. Additionally, it satisfies the high clarity and chromatic requirements in augmented reality displays [26, 27]. Such a film can be simply post-coated to the architectural glass as a diffractive-type solar concentrator. It is crucial to specifically optimize the design for a wide-angle, unidirectional and colorless transparency solar concentrator and ensure seamless coordination with the implementation of highly efficient solar capture that meets aesthetic standards and economic concerns.

Here, we propose a diffractive-type solar concentrator and demonstrate it by coating a specifically designed cholesteric liquid crystal (CLC) layer onto architectural glass. The CLC is a one-dimensional chiral photonic crystal, which selectively reflects incident light with the same handedness in the photonic band and allows the residual light to be transmitted directly. We stack a series of CLC layers of different helical pitches to extend the photonic band over the whole visible spectrum. Moreover, we preset a submicron-period lateral alignment to ensure that all visible light is diffracted and completely internally reflected over a wide-angle range. The diffracted light is unidirectionally concentrated to the edge of the architectural glass corresponding to the slant direction of the Bragg planes. For a normal incident, the average visible transmission (AVT) reaches 64.2% for visible light. A color rendering index (CRI) of 91.3 is obtained under these

conditions, and it remains greater than 85.5 at a view angle of $\pm 60^\circ$, perfectly matching the aesthetic standards. Owing to the circular polarization-dependent energy separation, up to 38.1% of the energy of the normally incident 532 nm laser is output from the objective edge of the architectural glass. The simulations further present the optical performance across $\pm 40^\circ$ incident angles, confirming the high energy concentration efficiency over a wide-angle range. We test the sunlight photovoltaic performance of a 1-inch-diameter prototype, which can directly drive a 10-mW fan outdoors. Furthermore, the CLC film can be seamlessly integrated with existing architectural glass and drastically reduces the number of required photovoltaic cells, offering a practical and cost-efficient approach for building integrated photovoltaic systems while adhering to aesthetic and economic considerations.

Results

Concept for a colorless and unidirectional solar concentrator (CUSC)

The sun is the main energy source for the Earth, supporting the existence and development of human beings. An electromagnetic wave is the dominant carrier for solar energy, which propagates at the speed of light. The transverse wave nature of light induces a polarization-dependent interaction with spatially periodic structures [28] (Fig. S1). Sunlight is inherently unpolarized, it can be equivalently decomposed to left- and right-handed circularly polarizations. CLC is a one-dimensional chiral photonic crystal. It selectively reflects the incidence circularly polarized light of the same handedness within the photonic band and transmits the residual light directly [29, 30]. The photonic band is expressed by the modified Bragg equation (Supplementary Note 1):

$$\Delta\lambda = (n_{\text{eff}} - n_o) \cdot P \cos(\theta + \alpha), \quad (1)$$

where $\Delta\lambda$ is the Bragg wavelength; n_{eff} , n_o represent the effective and ordinary refractive indices of the liquid crystal, separately; P is the helical pitch ($0-2\pi$) of the CLC; and θ and α are the incident angle of light and the tilt angle of the Bragg planes of the CLC, respectively. From the equation, the photonic band can be effectively broadened to the entire visible band via stacking a series of CLC layers of different P . To ensure a gap-free coverage across 400–750 nm, we numerically optimized pitches of the five-stacked layers inside the CLC for a continuous overlapping of the reflection bands (Supplementary Table 1). After such a CLC film is coated on architectural glass, a solar concentrator is formed, which can be seamlessly utilized in building integrated photovoltaic systems (Fig. 1a). With this design, when illuminated with AM 1.5G, the selected circular polarization located in the photonic band is reflected and transported to the edge of the glass via TIR (Fig. 1b, Fig. S2). The light escaping from the edge is captured by edge-mounted silicon-photovoltaic (Si-PV) cells. This design supplies a new integrated photovoltaic system for green buildings.

Optical properties of the CUSC

To ensure that the CUSC collects as much solar energy as possible, a multilayer CLC film with slanted Bragg planes is designed and fabricated. Circular polarization (CP) holography [31] is adopted to generate a submicron periodic alignment along the x -axis (Fig. 2a, Fig. S3). After sequentially coating CLCs with different chiral dopant

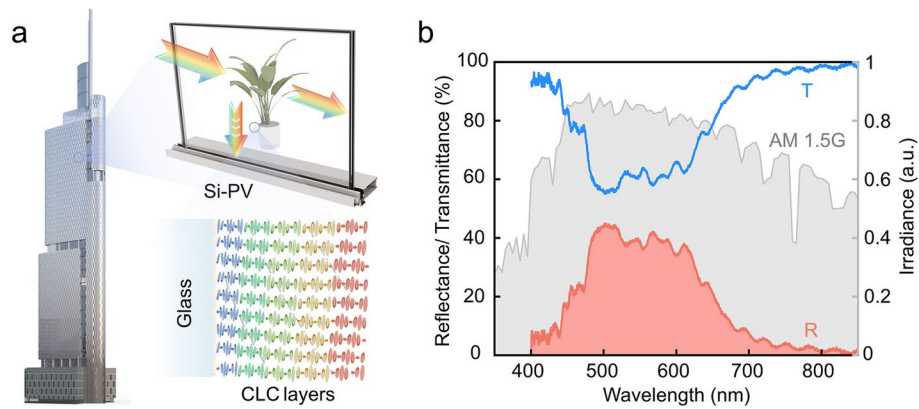


Fig. 1 Concept for a CUSC based on the circular-polarization splitting of the CLC layer-coated architectural glass. **a** (Left) Photo of Nanjing Zifeng Tower, the schemes for the CUSC integrated photovoltaic window (top-right) and stacked CLC layers of different helical pitches coated on architectural glass (bottom-right). **b** Transmittance (blue curve) and reflectance (red curve) of the CUSC under an AM 1.5G solar (grey curve). Si-PV: silicon photovoltaic; CLC layers: cholesteric liquid crystal layers; T: transmittance; R: reflectance

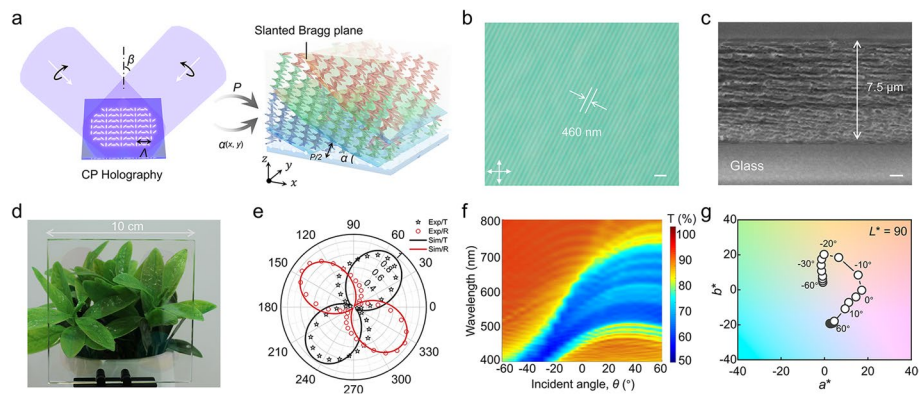


Fig. 2 Fabrications and characterizations of the CUSC. **a** Illustration for the photopatterning of laterally periodic CLC gratings and the 3D scheme for slanted Bragg planes inside the multilayered CLC of different P . **b** POM image of the CLC film with $\Lambda = 460$ nm. The scale bar indicates $1 \mu\text{m}$. **c** Cross-sectional SEM image of the multilayered CLC film with a thickness of $7.5 \mu\text{m}$. The scale bar indicates $1 \mu\text{m}$. **d** See-through photo of the CUSC ($10 \times 10 \text{ cm}^2$). **e** Dependencies of transmittance and reflectance on incident polarization at 530 nm . **f** Dependency of the photonic band on the incident angle θ . The color bar indicates that the transmittance varies from 50 to 100%. **g** CIELAB color space coordinates (a^* , b^*) corresponding to different incident angles with $L^* = 90$

concentrations (Supplementary Table 1) and separate UV polymerization, a multilayered CLC film with objective P is obtained. Owing to the guidance of the periodic alignment [32] in the submicron period (Λ) ($0-\pi$), slanted Bragg planes with tilt angle $\alpha = \sin^{-1}(P/2\Lambda)$ are formed as a result of the tilting of the CLC helical axes (Fig. 2a). According to the grating equation and the Bragg equation, $\Lambda = 460 \text{ nm}$ is the optimized value for achieving a wide-angle TIR across the entire visible spectrum. Λ is determined by the formula $\Lambda = \lambda_e / (2 \sin \beta)$, where λ_e is the wavelength for CP holography and 2β is the angle between two incident beams of opposite CPs. Here, we set $\lambda_e = 405 \text{ nm}$ and $2\beta = 52.3^\circ$. Under this condition, a large-area uniform grating is generated with $\Lambda = 460 \text{ nm}$ (Fig. 2b). The cross-sectional SEM image of the multilayered

CLC film reveals a slanted layered structure (Fig. 2c), which is consistent with the 3D illustration in Fig. 2a. The film thickness is 7.5 μm . We coat the CLC film onto commercial architectural glass ($10 \times 10 \text{ cm}^2$, Fig. 2d) and fabricate gratings in five 1-inch circular regions. Owing to the diffraction of light, these regions exhibit lower transmittance compared to grating uncovered areas. Notably, owing to their broad band diffraction characteristics, they are colorless and have no haze, making the greenery behind them clearly observable.

As human eyes are most sensitive to green light, we use 532-nm monochromatic light to characterize the CP-dependent energy division of the CUSC. Up to 38.1% of the energy propagates inside the architectural glass and is finally extracted from the objective single edge. To characterize the polarization dependency of the device, we rotate the fast axis of a quarter-wave plate to vary the incident polarization and record the intensities of the transmitted light and the light that escaped from the edge of the glass, accordingly. As revealed in Fig. 2e, an orthogonal CP separation between diffracted and transmitted light is exhibited (Supplementary Note 2), with maxima emerging at $55^\circ/145^\circ$ and $235^\circ/325^\circ$, respectively. The deviations compared to ideal normal reflection ($45^\circ/135^\circ$ and $225^\circ/315^\circ$) are attributed to the existence of slanted Bragg planes. We further characterize the incident angle θ -dependent transmittances in the range of 400–800 nm over $-60^\circ \leq \theta \leq 60^\circ$ (\pm for wave vector towards $x/-x$) (Fig. 2f). The AVT for normal incidence white light reaches 64.2%, whereas the value gradually reduces from 90.7% to 60.5% when θ changes from -60° to 60° [33]. The color shifts among different θ values are caused by incident angle-dependent photonic band variations (Figs. S3–S7). Figure 2g shows the CIELAB color space coordinates (a^* , b^*) corresponding to different incident angles when the lightness is fixed at $L^* = 90$. We can see that for most incident angles, the coordinates are located within a reasonable color tinting range ($-15 < a^* < 15$ and $-15 < b^* < 15$) for architectural glass [6, 34]. The performance can be improved via the stacking of more different P layers to further extend the photonic band. Therefore, the proposed diffractive-type solar concentrator is suitable for high transparency and wide-angle colorless photovoltaic integrated architectural glass.

Unidirectional waveguide

When normally illuminated by a collimated white flashlight, the CUSC asymmetrically diffracts the light to the $-x$ side edge of the architectural glass. Additionally, the light is spatially dispersed because of the diffraction caused by the short-period gratings (Fig. 3a). The unidirectional waveguide property is vividly verified by the top view image presented in the bottom left of Fig. 3a. Moreover, the logo of Nanjing University is clearly observed due to the high colorless transmittance of the CUSC. Additional details regarding RGB light incidence are provided in Fig. S8. We use Frank–Oseen elastic continuum model simulation to model the CUSC (Supplementary Note 3). A series of parallel slanted Bragg planes are calculated from the configuration of the multilayered CLC film. As revealed in Fig. 3b, the tilting angle α changes from 21° on the side adjacent to the glass to 30° on the opposite side. The propagation of diffracted light follows the diffraction equation below (Supplementary Note 4) [35]:

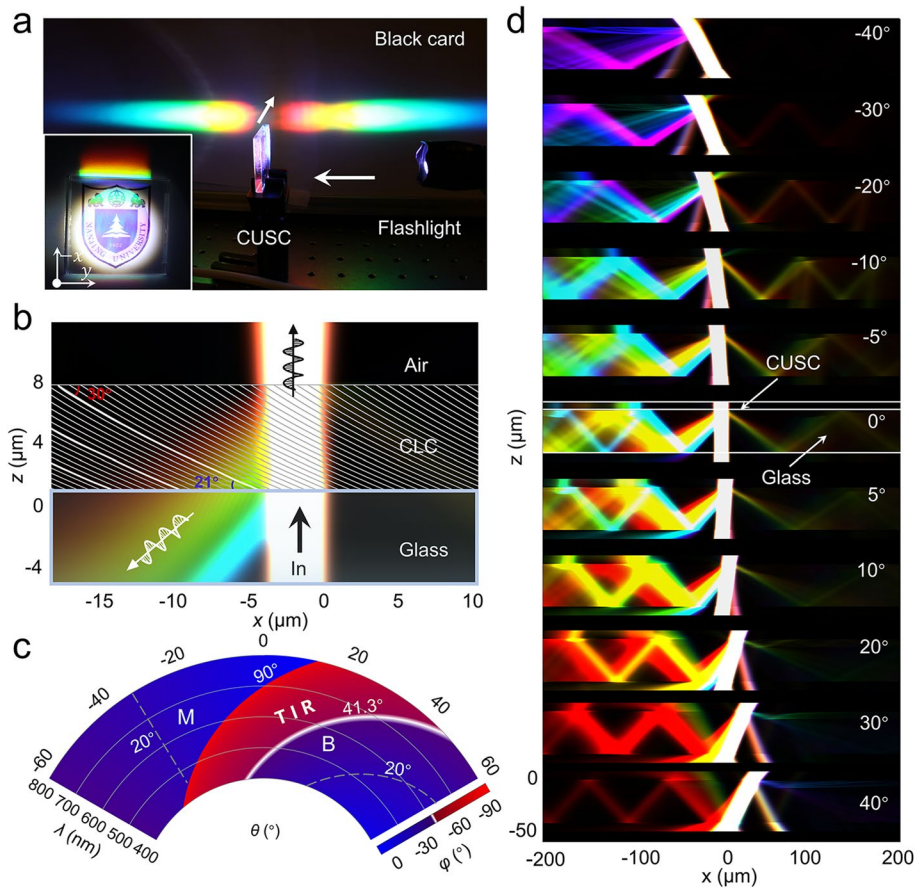


Fig. 3 Performances and simulations of the unidirectional waveguide. **a** The normally incident white light is asymmetrically diffracted to the $-x$ side edge of a $4 \times 4 \text{ cm}^2$ architectural glass. Inset shows a top view. **b** Simulations of the CP-dependent light division of the CUSC. **c** Dependencies of ϕ on θ and λ . The white line indicates that $\phi = \phi_c$. The color bar indicates that ϕ varies from 0° to -90° . **d** Unidirectional waveguide propagation of light inside the glass with θ varying from -40° to 40°

$$\begin{cases} n_g \sin(\phi) = n \sin(\theta) - \frac{\lambda}{\Lambda}, & \left| n \sin(\theta) - \frac{\lambda}{\Lambda} \right| \leq n_g \\ n_g \sin(\phi) = n \sin(\theta), & \left| n \sin(\theta) - \frac{\lambda}{\Lambda} \right| > n_g \end{cases} \quad (2)$$

where n and n_g are the refractive indices of the air and glass, respectively; λ represents the incident wavelength; and θ and ϕ are the incident angle in air and diffractive angle in glass (\pm for wave vector towards $x/-x$), respectively. The multilayered CLC exhibits broadband CP-selective Bragg reflection; only RCP light within the photonic band is reflected, and the light satisfying the TIR condition unidirectionally propagates in the glass waveguide (Fig. 3b, Supplementary Movie 1). Notably, the different wavelengths are diffracted by the separate CLC layers of different P . While the Bragg planes define the diffraction angle, light confinement is ultimately governed by the total internal reflection condition, which is key for the waveguide propagation.

We further simulate the θ -dependent diffraction of the CUSC. As shown in Fig. 3c, in the range of $-60^\circ \leq \theta < \theta_v$, where $\theta_v = \sin^{-1}(n_g - \lambda/\Lambda)$ and $n_g = 1.52$, the CLC film works as a waveplate instead of a grating; thus, the incident light is mirror reflected according to

$n_g \sin \phi = \sin \theta$ (Figs. S9–S11). As a result, the polarization state varies with changing film thickness (Fig. S12). When $\theta_t \leq \theta \leq 60^\circ$, the CLC film acts as a polarization volume grating with slanted Bragg planes. The results indicate that CP-selective reflection satisfies Eq. 2. The TIR condition is satisfied only when $|\phi| > \phi_c = \sin^{-1}(1/n_g)$. That is, only the cases located in the red region in Fig. 3c are transported in the waveguide and then captured at the edge of the glass. The detailed unidirectional waveguide performances are simulated and presented in Fig. 3d and Fig. S13. The central wavelengths redshift with θ varying from -60° to 60° , and broadband diffractions are exhibited at $-20^\circ \leq \theta \leq 20^\circ$. The simulations are all consistent with the results shown in Fig. 3c. The wide-angle broadband TIR ensures high concentrator efficiency for practical applications.

Photovoltaic performance and stability of the CUSC

A Si-PV cell ($0.5 \times 4 \text{ cm}^2$) is mounted on the escape edge of the light to form a CUSC-PV device ($4 \times 4 \times 0.5 \text{ cm}^3$ with a 1-inch-diameter active region), which can be considered a simple prototype for a CUSC-PV window. The excess cell area is marked by black tape to prevent the sun from directly illuminating the PV cell. The device drove a 10-mW fan under sunlight at 1 p.m. on July 1. After the sunlight was shielded, the fan stopped immediately (Fig. 4a, Supplementary Movie 2). Considering that the active area is just a 1-inch circular CLC grating, it vividly reveals the high energy conversion efficiency of the CUSC-PV cell. We systematically characterize the performance of the CUSC-PV device under AM 1.5G illumination [36, 37]. The optical efficiency (η) and power conversion efficiency (PCE) are calculated separately according to the following equations (Fig. S14) [38, 39]:

$$\eta = \frac{I_{SC} \cdot A'}{I_{SC} \cdot A}, \quad PCE = \frac{I_{SC} \cdot V_{OC} \cdot FF}{P_{in}}, \quad (3)$$

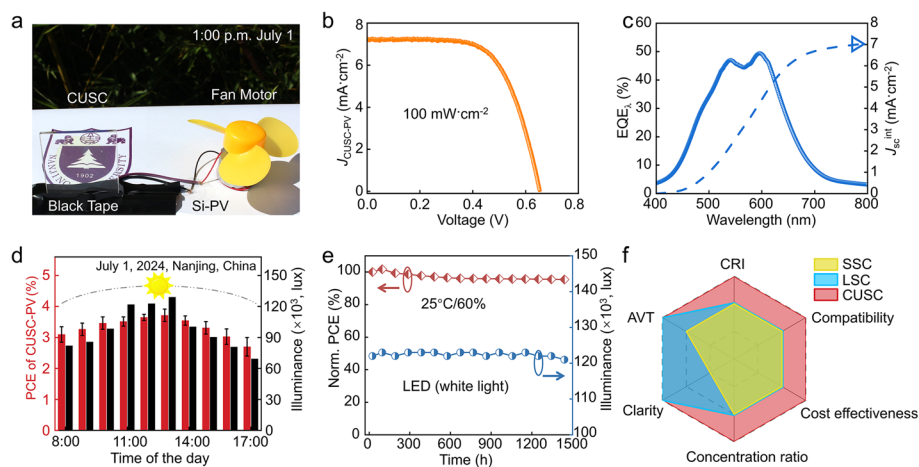


Fig. 4 Photovoltaic performance and stability of the CUSC. **a** The CUSC with an edge-mounted Si-PV cell drives a 10-mW fan under sunlight. **b** J - V characteristics of the CUSC-PV system under AM 1.5G illumination. **c** EQE spectra of the CUSCs. **d** Time-varying PCE of a CUSC-PV system and the corresponding illuminance during a day under natural sunlight irradiation. **e** Stability test on CUSC-PVs (red quads) under white LED irradiation (blue circles) at 25 °C and 60% humidity. **f** Comparisons of key performance metrics among SSC, LSC and CUSC. SSC: scattering solar concentrator; LSC: luminescent solar concentrator

where I_{SC} and I'_{SC} are the short-circuit currents of the CUSC-PV and the PV cell under AM 1.5G illumination, A and A' are the areas of the CUSC and its light escaping edge, respectively; $J_{SC}=I_{SC}/A$ is the current density; V_{OC} is the open-circuit voltage; FF is the fill factor of the CUSC-PV; and P_{in} is the irradiation intensity. Figure 4b presents a J of $7.0 \pm 0.2 \text{ mA cm}^{-2}$, a V_{OC} of $0.65 \pm 0.01 \text{ V}$, and an FF of $80 \pm 1\%$. Accordingly, $\eta = 18.1 \pm 0.1\%$, and $PCE = 3.7 \pm 0.1\%$ (additional details can be found in Fig. S15 and Supplementary Table 2). The measured position-average external quantum efficiency (EQE) is consistent with the photonic band of the CUSC-PV (Fig. 4c), and the integrated short-circuit current density (J_{SC}^{int}) matches well with the J_{SC} extracted from the J - V characteristics presented in Fig. 4b.

We tested the time-varying PCE of the CUSC-PV cell and corresponding illuminance outdoors in Nanjing, China, at 8:00 AM – 5:00 PM on July 1, 2024. The PCE changed from 3.1% to 3.7% (maximum) to 2.7% under sunlight illuminance varying from 82 to 129 klux to 69 klux (Fig. 4d), which maintained a high value all day. The long-term stability was also verified. A total of 95.4% of the PCE peak value was maintained even after 1,500 h of white LED illumination under ambient conditions (25 °C, 60% humidity) (Fig. 4e). Under practical conditions, sunlight first passes through the architectural glass, which efficiently blocks harmful UV light, protecting the CLC film from aging and yellowing. The CLC can be coated to a polymer film and attached to the indoor side of an architectural glass instead for mechanical protection, which ensures a long-term durability. Figure 4f presents a radar chart of the performance comparisons among SSC, LSC and CUSC (Fig. S16 and Supplementary Table 3–4). Obviously, the CUSC is superior to the other two in terms of all the metrics. Owing to the unique colorless and unidirectional waveguiding of the CUSC, excellent CRI (91.3) and clarity, as well as a higher AVT (64.2%) and concentration ratio, are exhibited. The CLC multilayers can be easily coated or transferred to glass, and only the light escaping edge needs to be modified to mount a PV cell (75% photovoltaic cell reduction). These advantages enable seamless integration with existing architectural windows with significant cost efficiency.

Discussion and conclusion

We propose a diffractive-type solar concentrator, which enables wide-angle, colorless and unidirectional light capture on the basis of stacked CLC layers of optimized helical pitches and submicron-period lateral alignments. Owing to the broad-band CP separation, the CUSC has a CRI of 91.3 and an AVT of 64.2% for normally incident light, and 18.1% of the total incidence energy is confined inside the architectural glass and finally escapes from the objective edge. In other word, the CUSC exhibits high solar concentration capability while maintaining excellent transparency and aesthetic quality. High performance can be guaranteed over a wide incident angle range. Notably, the concentration ratio exceeds 1 when $L/d=8$. For a typical window composed of two meters wide and 0.5 cm thick glass, the ratio reaches 50, indicating the high performance of the CUSC-PVs. Owing to the ultrahigh concentration ratio and 75% reduction in the number of photovoltaic cells due to unidirectional diffraction, high-performance but expensive PV cells, such as gallium arsenide PVs, can be adopted to further increase the PCE.

The CUSC can be seamlessly integrated with architectural glass by simply coating cascaded CLC films. This approach is superior to existing approaches, especially

in terms of aesthetic quality and economic viability. Though the prototype with a 1-inch-diameter active region directly drives a 10-mW fan, clearly revealing the great potential of CUSC-PVs. To scale up production, several improvements in materials and procedures need to be considered: (1) optimization on the CLC thickness, helical pitch and lateral period to increase both the reflectance and the photonic bandgap; (2) CLC films of opposite helical handedness can be integrated to further increase the PCE; and (3) development of roll-to-roll photopatterning for uniform, large-area fabrication. Although polymeric CLCs are intrinsically stable, UV-induced polymer aging and yellowing still need to be avoided to ensure the long-term durability under outdoor conditions. To reduce polarization dependent leakage in large-area waveguides, phase retarders should be introduced to properly control the circular polarizations inside the waveguide [35]. The promising CUSC design would be widely adopted in green buildings, agricultural photovoltaics and other emerging areas, matching well with the rapid urbanization and sustainable development of our society. It is expected to contribute to a global terawatt-scale green energy supply and reduce annual carbon emissions by billions of tons (Supplementary Note 5) [40].

Materials and methods

Materials

The photoalignment agent sulfonic azo dye SD1 (NCLCP, China) is dissolved in N,N-dimethylformamide at 0.3 wt%. The CLC mixture of the reactive mesogen RM257 (NCLCP, China), the chiral dopant R5011 (NCLCP, China), the photoinitiator Omnirad651 (BASF, Germany) and the surfactant Zonyl8857A (DuPont, USA) is solved in propylene glycol methyl ether acetate (PGMEA). The helical twisting power of R5011 in RM257 is $108 \mu\text{m}^{-1}$ at room temperature. The concentration of R5011 in the precursor is adjusted to control the helical pitch of the CLC. The detailed weight ratios of the different constituents are presented in Supplementary Table 1. Architectural glass (Luoyang Guluo, China), norland optical adhesive 68 (Norland, USA), high-tack adhesive tape (3 M, USA) and strip Si-PV cells (Sunpower, USA) are all commercially purchased.

Fabrications

The ultrasonically cleaned architectural glass ($10 \times 10 \times 0.5 \text{ cm}^3$ or $4 \times 4 \times 0.5 \text{ cm}^3$) is spin-coated with SD1 solution at 800 rpm for 5 s and subsequently at 3000 rpm for 40 s and then annealed at 100°C for 10 min. The photoalignment film is exposed at a dose of 5 J cm^{-2} by circular-polarization holography with the setup shown in Fig. S3. A single-longitudinal-mode laser (DLC HOLO-LITHO 405, Toptica, Germany) is adopted as the light source. The pitch-varied CLC layers are spin-coated for fourteen separate times, and the detailed processing parameters are presented in Supplementary Table 1. Each layer is UV cured (365 nm , 3 J cm^{-2}) in a nitrogen environment before the coating of the subsequent layer. Finally, a NOA 68 film is coated onto the top layer and UV cured to protect the CLC film. A 0.5 cm wide Si-PV cell is affixed to the edge of the CUSC via high-adhesive transparent tape, and the excess areas are masked by black tapes.

Characterizations

Photographs are captured under the reflective mode of a polarization optical microscope (Nikon 50i POL, Japan). Cross-sectional scanning electron microscopy (SEM) images are recorded via a field-emission scanning electron microscope (SEM MERLIN, Carl Zeiss, Germany). The angle-dependent reflectance/transmittance spectra of the CUSC are measured by an angular resolution spectral system (R1, Ideaoptics, China), where a standard aluminum mirror acts as an ideal reflector reference. The CP-dependent energy division of the CUSC is characterized by a coherent continuous wave laser with a wavelength of 532 nm (JCOPTIX, China). The digital photographs are taken with a digital camera (EOSM, Canon, Japan). The total incidence and edge-transmitted power density from the CUSC are tested by an optical power meter (Thorlabs, USA). The photon flux of the light source is measured by a luminance meter (LS-160, China).

The J – V characteristics of the CUSC-PV device and the Si-PV are measured via a Keithley 2400 source meter over a voltage range of -0.2 V to 1.2 V in 0.04 V increments. Illumination (100 mW cm^{-2} , AM 1.5 Global) is provided by a solar simulator (94023A, Newport, USA). The short-circuit current (I_{SC}) and open-circuit voltage (V_{OC}) under direct sunlight are recorded via digital multimeters (Fluke, USA). The external quantum efficiency (EQE) is measured at zero bias via an electrochemical workstation (Zahner, Germany) equipped with a chopper and TLS-03 monochromator spanning 365–1000 nm, as schematically illustrated in Fig. S14.

Numerical simulations

We simulate the configuration of the LC director via the Frank–Oseen elastic continuum model (Supplementary Note 3). The finite-difference time-domain (FDTD) simulations are performed via Ansys Lumerical FDTD software to analyze the optical properties of the CUSC on the basis of the LC director configurations. In the simulations, the ordinary and extraordinary refractive indices of the LC are set as $n_o = 1.508$ and $n_e = 1.678$, respectively. The propagation of light in the range of 400–800 nm within the CUSC is systematically simulated. The simulated optical fields are computationally overlaid with corresponding colors. Far-field diffraction analysis is employed to determine the reflection and dispersion characteristics.

Abbreviations

CLC	Cholesteric liquid crystal
CUSC	Colorless and unidirectional solar concentrator
TIR	Total internal reflection
AVT	Average visible transmission
CRI	Color rendering index
PV	Photovoltaic

Supplementary Information

The online version contains supplementary material available at <https://doi.org/10.1186/s43074-025-00178-3>.

Supplementary Material 1.

Supplementary Material 2: Movie S1. Wavelength dependent diffraction inside the CUSC.

Supplementary Material 3: Movie S2. A CUSC-PV device ($4 \times 4 \times 0.5 \text{ cm}^3$) powering a 10 mW fan motor under sunlight.

Acknowledgements

Not applicable.

Authors' contributions

W. Hu and Y. Lu guided the project. D. Zhang, Z. Guo and W. Hu conceived the idea and designed the experiment. D. Zhang, Z. Guo, C. Xu, and J. Li performed the experiments and measurements. W. Hu revised and submitted the manuscript. All authors analyzed the experimental data, drew the figures and prepared the manuscript. All authors read and approved the final manuscript.

Funding

This work was supported by the National Key Research and Development Program of China (2022YFA1203700), the National Natural Science Foundation of China (NSFC) (T2488302, 62035008 and 62405129), and the Natural Science Foundation of Jiangsu Province (BK20233001).

Data availability

The data that support the findings of this study are available from the corresponding author upon reasonable request.

Declarations**Ethics approval and consent to participate**

Not applicable.

Consent for publication

All authors agree with the publication.

Competing interests

The authors declare no competing interests.

Received: 14 May 2025 Revised: 11 June 2025 Accepted: 15 July 2025

Published online: 28 July 2025

References

1. Bloom DE, Canning D, Fink G. Urbanization and the wealth of nations. *Science*. 2008;319(5864):772–5.
2. Nethercote M. Theorising vertical urbanisation. *City*. 2018;22(5–6):657–84.
3. Huang X. The small-drone revolution is coming – scientists need to ensure it will be safe. *Nature*. 2025;637:29–30.
4. Zhao X, Zhong Z, Lu X, Yu Y. Potential greenhouse gas risk led by renewable energy crowding out nuclear power. *iScience*. 2022;25(2):103741.
5. AsadiAghajari H, Niknam T, Shasadeghi M, Sharifhosseini SM, Taabodi MH, Sheybani E, et al. Analyzing complexities of integrating renewable energy sources into smart grid: a comprehensive review. *Appl Energy*. 2025;383:125317.
6. Traverse CJ, Pandey R, Barr MC, Lunt RR. Emergence of highly transparent photovoltaics for distributed applications. *Nat Energy*. 2017;2(11):849–60.
7. Xue Q, Xia R, Brabec CJ, Yip H-L. Recent advances in semi-transparent polymer and perovskite solar cells for power generating window applications. *Energy Environ Sci*. 2018;11(7):1688–709.
8. Shao Z, Huang A, Cao C, Ji X, Hu W, Luo H, et al. Tri-band electrochromic smart window for energy savings in buildings. *Nat Sustain*. 2024;7(6):796–803.
9. Marchini F, Chiatti C, Fabiani C, Pisello AL. Development of an innovative translucent–photoluminescent coating for smart windows applications: an experimental and numerical investigation. *Renew Sust Energy Rev*. 2023;184:113530.
10. Nayak PK, Mahesh S, Snaith HJ, Cahen D. Photovoltaic solar cell technologies: analysing the state of the art. *Nat Rev Mater*. 2019;4(4):269–85.
11. Nagaraja MR, Biswas WK, Selvan CP. Advancements and challenges in solar photovoltaic technologies: enhancing technical performance for sustainable clean energy – a review. *Sol Energy Adv*. 2025;5:100084.
12. McKenna BC, Evans R. Towards efficient spectral converters through materials design for luminescent solar. *Adv Mater*. 2017;29:1606491.
13. Debije MG, Verbunt PPC. Thirty years of luminescent solar concentrator research: solar energy for the built environment. *Adv Energy Mater*. 2011;2(1):12–35.
14. Huang S, Guo H, Xia P, Sun H, Lu C, Feng Y, et al. Integrated device of luminescent solar concentrators and electrochromic supercapacitors for self-powered smart window and display. *Nat Commun*. 2025;16(1):2085.
15. Meinardi F, Ehrenberg S, Dharmo L, Carulli F, Mauri M, Bruni F, et al. Highly efficient luminescent solar concentrators based on earth-abundant indirect-bandgap silicon quantum dots. *Nat Photonics*. 2017;11(3):177–85.
16. You Y, Tong X, Imran Channa A, Zhi H, Cai M, Zhao H, et al. High-efficiency luminescent solar concentrators based on composition-tunable eco-friendly core/shell quantum dots. *Chem Eng J*. 2023;452:139490.
17. Chen R-T, Chau JLH, Hwang G-L. Design and fabrication of diffusive solar cell window. *Renew Energy*. 2012;40(1):24–8.
18. Jin C, Feng C, Chen Y, Zhang T, He H, Na H, et al. Fabricating a scattering–fluorescent luminescent solar concentrator synchronously to achieve broad-spectrum solar energy utilization and light pollution inhibition. *Energy Environ Sci*. 2024;17(16):5931–40.
19. Liu X, Gädeke F, Hohgardt M, Walla PJ. Highly efficient and stable luminescent solar concentrator based on light-harvesting and energy-funneling nanodot pools feeding aligned, light-redistributing nanorods. *Sol RRL*. 2024;8(18):2400273.

20. Liu X, Benetti D, Liu J, Jin L, Rosei F. Color-tunable multilayered laminated luminescent solar concentrators based on colloidal quantum dots. *Nano Energy*. 2023;111:108438.
21. Zhang B, Lyu G, Kelly EA, Evans RC. Förster resonance energy transfer in luminescent solar concentrators. *Adv Sci*. 2022;9(23):2201160.
22. Xia P, Sun H, Guo H, Zhao K, Liang C, Lu C, et al. Luminescent solar concentrator with advanced structure for reabsorption loss suppression and synergistic energy harvesting. *Adv Funct Mater*. 2024;34:2401124.
23. de Clercq DM, Chan SV, Hardy J, Price MB, Davis NJLK. Reducing reabsorption in luminescent solar concentrators with a self-assembling polymer matrix. *J Lumin*. 2021;236:118095.
24. Ding Y, Yang Q, Li Y, Yang Z, Wang Z, Liang H, et al. Waveguide-based augmented reality displays: perspectives and challenges. *eLight*. 2023;3(1):1–24.
25. Rafayelyan M, Brasselet E. Spin-to-orbital angular momentum mapping of polychromatic light. *Phys Rev Lett*. 2018;120(21):213903.
26. Xiong J, Hsiang EL, He Z, Zhan T, Wu ST. Augmented reality and virtual reality displays: emerging technologies and future perspectives. *Light Sci Appl*. 2021;10(1):216.
27. Xiong J, Wu ST. Planar liquid crystal polarization optics for augmented reality and virtual reality: from fundamentals to applications. *eLight*. 2021;1(1):1–20.
28. Yu N, Genevet P, Kats MA, Aletta F, Tetienne JP, Capasso F, Gaburro Z. Light propagation with phase discontinuities: generalized laws of reflection and refraction. *Science*. 2011;334(6054):333–7.
29. Kobashi J, Yoshida H, Ozaki M. Planar optics with patterned chiral liquid crystals. *Nat Photonics*. 2016;10(6):389–92.
30. Barboza R, Bortolozzo U, Clerc MG, Residori S. Berry phase of light under bragg reflection by chiral liquid-crystal media. *Phys Rev Lett*. 2016;117(5):053903.
31. Zhang D, Xu C-T, Chen Q-M, Cao H, Yu H-G, Tan Q-G, et al. Cascaded chiral birefringent media enabled planar lens with programable chromatic aberration. *Photonix*. 2024;5(1):17.
32. Chigrinov VG, Kozenkov VM, Kwok HS. Photoalignment of liquid crystalline materials: physics and applications. Chichester, UK: Wiley; 2008.
33. Yang C, Liu D, Bates M, Barr MC, Lunt RR. How to accurately report transparent solar cells. *Joule*. 2019;3(8):1803–9.
34. Yang C, Sheng W, Moemeni M, Bates M, Herrera CK, Borhan B, et al. Ultraviolet and near-infrared dual-band selective-harvesting transparent luminescent solar concentrators. *Adv Energy Mater*. 2021;11(12):2003581.
35. Ding Y, Gu Y, Yang Q, Yang Z, Huang Y, Weng Y, et al. Breaking the in-coupling efficiency limit in waveguide-based AR displays with polarization volume gratings. *Light Sci Appl*. 2024;13(1):185.
36. Yang C, Atwater HA, Baldo MA, Baran D, Barile CJ, Barr MC, et al. Consensus statement: Standardized reporting of power-producing luminescent solar concentrator performance. *Joule*. 2022;6(1):8–15.
37. Debije MG, Evans RC, Griffini G. Laboratory protocols for measuring and reporting the performance of luminescent solar concentrators. *Energy Environ Sci*. 2021;14(1):293–301.
38. Li J, Zhao H, Zhao X, Gong X. Boosting efficiency of luminescent solar concentrators using ultra-bright carbon dots with large Stokes shift. *Nanoscale Horiz*. 2023;8(1):83–94.
39. Zhou Y, Benetti D, Fan Z, Zhao H, Ma D, Govorov AO, et al. Near infrared, highly efficient luminescent solar concentrators. *Adv Energy Mater*. 2016;6(11):1501913.
40. Meinardi F, Bruni F, Brovelli S. Luminescent solar concentrators for building-integrated photovoltaics. *Nat Rev Mater*. 2017;2(12):17072.

Publisher's Note

Springer Nature remains neutral with regard to jurisdictional claims in published maps and institutional affiliations.